Characterization of thin metal films via frequency-domain thermoreflectance

Aaron J. Schmidt,[1,2,a)] Ramez Cheaito,[2] and Matteo Chiesa[2]
[1]*Department of Mechanical Engineering, Massachusetts Institute of Technology Cambridge, Massachusetts, USA*
[2]*Department of Mechanical Engineering, Masdar Institute of Science and Technology, Abu Dhabi, United Arab Emirates*

(Received 30 October 2009; accepted 12 December 2009; published online 27 January 2010)

Frequency-domain thermoreflectance is extended to the characterization of thin metals films on low thermal diffusivity substrates. We show how a single noncontact measurement can yield both the thickness and thermal conductivity of a thin metal film with high accuracy. Results are presented from measurements of gold and aluminum films 20–100 nm thick on fused silica substrate. The thickness measurements are verified independently with atomic force microscope cross sections, and the thermal conductivity measurements are verified through electrical conductivity measurements via the Wiedemann–Franz law. The thermoreflectance thermal conductivity values are in good agreement with the Wiedemann–Franz results for all the films at least 30 nm thick, indicating that our method can be used to estimate electrical conductivity along with thermal conductivity for sufficiently thick films. © *2010 American Institute of Physics*. [doi:10.1063/1.3289907]

I. INTRODUCTION

Thin metal films are essential for a vast array of technologies in optics and microelectronics. The thickness, density, thermal conductivity, and electrical conductivity of these films are all critical parameters affecting their performance in a given application. As a result, numerous techniques have been developed to characterize these properties. Of particular interest are noncontact methods, due to their nondestructive nature and the ease with which they can be incorporated into manufacturing processes.

Many of the methods that have been developed are based on photothermal phenomena. These fall into the categories of frequency-domain methods based on a modulated laser heating source,[1–8] and time-domain methods based on the sample response to a short laser pulse, such as time-domain thermoreflectance (TDTR).[9–12] Recently, the authors have introduced a frequency-domain thermoreflectance (FDTR) method[13] that combines some of the advantages of TDTR, such as good sensitivity for submicron thin films and a straightforward coaxial laser spot geometry, with the advantages of modulated photothermal methods, such as relative experimental simplicity due to lack of a moving delay stage and the ability to explore a range of thermal penetration depths with a single measurement.

In this work, we show how FDTR can be applied to thin metal films on low thermal diffusivity substrates such as glass or quartz. We simultaneously determine the thickness or density of a metal film, and the film thermal conductivity. From the thermal conductivity, we can obtain the electrical conductivity through the well-known Wiedemann–Franz (WF) law.[14]

Separately, each of these topics has been addressed with various methods. Film thickness, for example, can be determined by profilometry, by picosecond acoustics provided the sample has a strong thermoelastic response,[15] or with a modulated thermal wave approach.[5] Techniques for measuring the thermal conductivity in thin metal films are less common. These include scanning probe techniques such as scanning Joule microscopy,[16] and photothermal methods where a probe laser spot is moved over a pump laser spot and a three-dimensional thermal model is used to determine film conductivity based on the signal phase as a function of the spot separation.[3,8,17]

Our FDTR approach has several advantages. The measurement geometry—coaxial laser spots passed through a single objective lens—allows for simple alignment and a straightforward two-dimensional analytical thermal model. Additionally, because the measurement covers a wide frequency range, the sensitivity to film thermal mass and thermal conductivity separate into different transport regimes, allowing both properties to be determined simultaneously. Thus, from a single noncontact measurement we obtain the critical structural and transport properties of the metal film.

II. BACKGROUND

A complete description of the FDTR method can be found in.[13] The essential features are that a modulated laser heating source, called the pump beam, impinges on a sample, while a second, unmodulated beam is reflected off the sample and directed into a photodetector. Both pump and probe beams are coaxially directed through a single microscope objective and focused to spots 10–20 μm in diameter. The laser beams can be pulsed or continuous-wave (cw). In the case of pulsed beams, the pump and probe beams typically originate from the same laser and are divided with a beamsplitter. An optical delay separates the pump and probe pulses by a time τ.

If the sample is a metal film on a substrate, the incoming pump light is absorbed by the film and converted into heat. The reflectivity is in turn proportional to the film surface temperature. The phase and amplitude response of the probe

a)Electronic mail: aarons@.mit.edu.

 © 2010 American Institute of Physics

Downloaded 26 Sep 2011 to 65.96.249.255. Redistribution subject to AIP license or copyright; see http://jap.aip.org/about/rights_and_permissions

beam at the modulation frequency are recorded by a lock-in amplifier while the frequency is swept over a range such as 50 kHz–20 MHz. The frequency response can be expressed as a complex number $Z(\omega_0)$ such that the output of the lock-in amplifier for a reference wave $e^{i\omega_0 t}$ is given by

$$Ae^{i(\omega_0 t+\phi)} = Z(\omega_0)e^{i\omega_0 t}, \quad (1)$$

where ϕ is the phase, A is the amplitude, and ω_0 is the modulation frequency. In the case of a pulsed laser, the quantity $Z(\omega_0)$ is related to the properties of the sample through[11,18]

$$Z(\omega_0) = \beta \sum_{k=-\infty}^{\infty} H(\omega_0 + k\omega_s)e^{ik\omega_s \tau}, \quad (2)$$

where $H(\omega_0)$ is the thermal frequency response of the sample weighted by the intensity of the probe beam, and β is a factor including the thermoreflectance coefficient of the metal film and the power in the pump and probe beams. This result assumes the sample responds as a linear system and behaves as a continuum; these conditions are usually met for small temperature excursions and delay times greater than $\sim$100 ps. For the case of cw lasers, we have simply

$$Z(\omega_0) = \beta H(\omega_0). \quad (3)$$

The sample frequency response, $H(\omega_0)$, is analytically obtained by solving the heat diffusion equation for a Gaussian heat source (the pump beam) impinging on a multilayer stack of materials and weighting the resulting temperature distribution at the top surface by the Gaussian intensity distribution of the probe beam. A full treatment of this problem can be found elsewhere[11,18] and we do not repeat the theory here. Each material layer in the sample has a thickness, specific heat capacity, cross-plane thermal conductivity, and in-plane thermal conductivity. In addition, between each layer there is a thermal boundary conductance, so in total for a sample with n layers there are $5n-1$ physical properties.

In our measurements, we treat the phase of the lock-in signal as the observable quantity. Since we are using a pulsed laser system, this is the phase of Eq. (2). The measurement of individual physical properties is performed as an inverse problem, minimizing the error between the lock-in phase data and the phase of Eq. (2) or Eq. (3) via a nonlinear least-squares algorithm. Typically one to three properties can be determined from a single measurement.[13]

Our FDTR implementation is based on a Ti:sapphire laser which emits a train of 150 fs long pulses at a repetition rate of 80 MHz. The center wavelength is 815 nm and the power per pulse is roughly 15 nJ. Each pulse is split into pump and probe pulses, and the probe pulses are delayed relative to the pump pulses by 500 ps. The $1/e^2$ beam radii are 10 μm for the pump beam and 3.5 μm for the probe beam. This system was used to generate all the data presented in this work. More details on our setup are given elsewhere.[19]

III. RESULTS AND DISCUSSION

Measurements were performed on a series of Au and Al films sputtered onto fused silica substrates with thickness in the range 20–100 nm. The films were deposited at a pressure of 3 mT. All measurements were performed in air at atmospheric pressure and a temperature of approximately 22 °C. Film thickness and thermal conductivity were determined from the signal phase data using a nonlinear least-squares routine. Such routines typically require an initial guess to determine the values of the free parameters that minimize the error between the model and data. In order to gauge the robustness of our results, we used several initial guesses for both parameters varying them by up to an order of magnitude and verified that the routine always returned the same set of best fit values. We assumed isotropic thermal conductivities for both the film and the substrate during fitting, although as we discuss later, the measurement is insensitive to the cross-plane thermal conductivity of the metal film, so in effect we are only determining the in-plane film thermal conductivity. Thermal anisotropy in the substrate (such as quartz for example) will impact the measurement and in such a case both in-plane and cross-plane substrate thermal conductivities should be put into the thermal model.

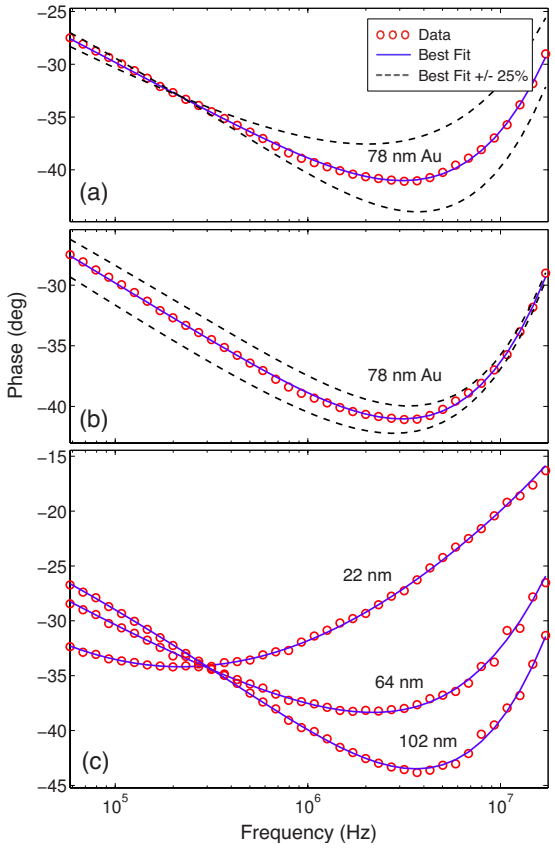

FIG. 1. (Color online) (a) Sample data and the best fit curve for a sample of 78 nm Au on a fused silica substrate. Also shown are the curves obtained by varying the Au thickness by ±25%. (b) The same data, this time with the film thermal conductivity varied ±25%. (c) Sample data and best fit curves for Au layers 22, 64, and 102 nm thick.

In Fig. 1 we plot sample data and best fit curves from Au films sputtered onto a fused silica substrate. In Fig. 1(a), data and the best fit curve for an 80 nm thick Au film are shown. Also shown are solutions obtained by varying the thickness of the metal layer by ±25%. In Fig. 1(b), the same data and the best fit curve are shown, but this time the metal thermal

Downloaded 26 Sep 2011 to 65.96.249.255. Redistribution subject to AIP license or copyright; see http://jap.aip.org/about/rights_and_permissions

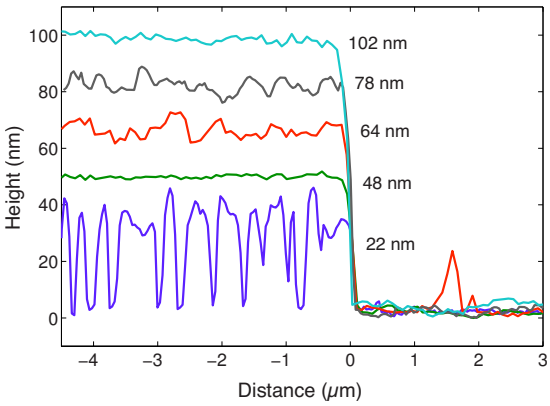

FIG. 2. (Color online) AFM cross sections for the gold films in this study. The thinnest film exhibited agglomeration and was much less smooth than the others; mean thickness was approximately 22 nm.

conductivity is varied ±25%. In this case the solutions converge at high frequency where lateral transport is negligible. Finally in Fig. 1(c) data and fits from 22, 64, and 102 nm Au films are shown. We obtained similarly good fits for 30–100 nm Al films on fused silica.

At least five measurements were made on several Al and Au films 20–100 nm thick, and the values for film thermal conductivity and thickness were obtained simultaneously. In our calculations, we assumed typical thermal interface conductances of 150 and 75 $MW/m^2\,K$ for the Al/fused silica boundary and Au/fused silica boundary, respectively, although as we explain later, sensitivity analysis shows that changing these has a negligible impact on the result.

Film thicknesses were independently determined using multiple atomic force microscope (AFM) cross sections of scratched regions (Asylum Research, MFP-3D system). A sample of the cross-sectional images are shown in Fig. 2. The 22 nm thick Au film showed signs of agglomeration and the films was not smooth; in this case the mean value was taken as the thickness. In Fig. 3, the thickness values determined via FDTR are plotted against the AFM values and the two sets are in good agreement. We have assumed the density of the bulk metals in determining film thickness; as we discuss later, if the film properties deviate from bulk properties, this will lead to an error.

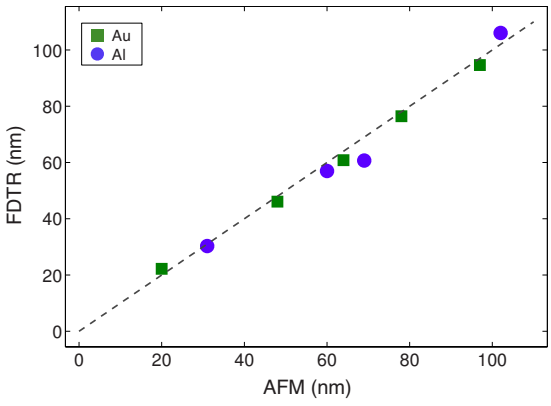

FIG. 3. (Color online) Film thickness data obtained for Au and Al films on fused silica substrates. The ordinate is the thickness determined from AFM cross sections while the abscissa is the FDTR value. Error bars based on two standard deviations are approximately the size of the symbols used.

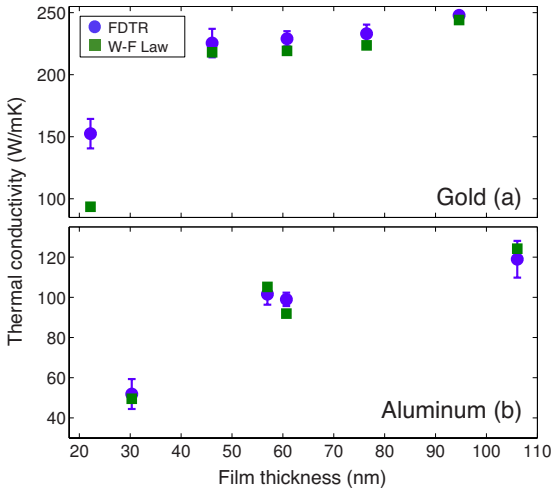

FIG. 4. (Color online) Thermal conductivity data obtained for (a) Au and (b) Al films on fused silica substrates. Circles are values obtained with the FDTR method, while the squares are values computed from electrical conductivity measurements using the WF law.

Two sets of room-temperature film thermal conductivity data are shown in Fig. 4 for (a) gold and (b) aluminum. The first set (circles) was obtained via FDTR simultaneously with the thickness data shown in Fig. 3. The error bars indicate two standard deviations based on five to six measurements at different locations on the sample. The generally larger error bars for the thinner films reflect the fact that thinner films transport less heat and therefore make the measurement less sensitive. The second set of measurements (squares) are obtained from electrical conductivity measurements via the WF law, which states

$$k/\sigma = LT, \tag{4}$$

where k is the thermal conductivity, σ is the electrical conductivity, T is the temperature, and L is the Lorenz number. Electrical conductivity measurements were obtained via the van der Pauw method using a Hall effect measurement system (Lakeshore model 7604), and the thermal conductivity was then determined using the experimentally determined Lorenz numbers for Al and Au.[14]

The thermal conductivities obtained directly from FDTR and indirectly via the electrical conductivity are in good agreement, with a discrepancy of 1%–5%. The notable exception is the 22 nm Au film, where the measured thermal conductivity is 40% higher than the value predicted by the WF law. Similar findings at room temperature have been reported in films of platinum[20] and gold[21] thinner than 30 nm, where it is believed that grain boundary scattering effects reduce the electrical conductivity more than the thermal conductivity. At low temperatures the effect is amplified, since the carrier wavelengths become longer compared to grain size.

There are other plausible explanations for the deviation from the WF law. As is clear from Fig. 2, the morphology of the 22 nm gold film is not smooth, and there are multiple heat paths through the film. These include near field radiation in the gaps, electron tunneling, and molecular air conduction through gaps. There are also multiple electron and phonon

Downloaded 26 Sep 2011 to 65.96.249.255. Redistribution subject to AIP license or copyright; see http://jap.aip.org/about/rights_and_permissions

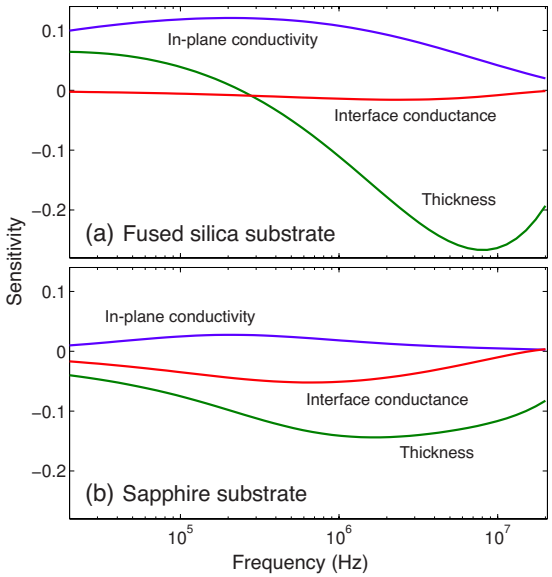

FIG. 5. (Color online) (a) The sensitivity parameter, Eq. (5), for in-plane thermal conductivity, metal-substrate boundary conductance, and metal thickness, for a sample consisting of an 80 nm film of Au deposited on a fused silica substrate. (b) The same sensitivities, calculated for a sapphire substrate. The phase angle in Eq. (5) is taken in radians.

scattering mechanisms. All these effects will depend on the detailed morphology of the film. In addition, because the Au film was both soft and very thin, making contact for the electrical measurements was challenging, and despite our careful attempts it is possible that poor contact is causing the lower apparent electrical conductivity.

Because our FDTR approach measures the total in-plane thermal conductivity while electrical measurements give only the electronic contribution, we believe that combining FDTR with electrical measurements in carefully designed experiments could isolate some of the transport mechanisms and shed light on the details of the transport physics in very thin metal films. We are planning on addressing some of these issues in a future work.

It is useful to consider the sensitivity of the measurement to various parameters of interest. We define the sensitivity of the measurement to a property x as

$$S_x = d\phi/d \ln x, \tag{5}$$

where we take the phase in radians. We consider an 80 nm film of Au deposited on a fused silica substrate, Fig. 5(a), and sapphire substrate, Fig. 5(b), and plot the sensitivity to film thickness, lateral thermal conductivity, and the metal-substrate boundary conductance.

At high frequencies, the thermal penetration depth, given by $\sqrt{2\alpha/\omega_0}$ where α is the substrate thermal diffusivity and ω_0 is the modulation frequency, is small compared to the spot radii, and transport approaches the one-dimensional situation. In this case, sensitivity to in-plane thermal conductivity is low. Sensitivity to cross-plane thermal conductivity, not shown, is essentially zero because there is no significant temperature gradient across the film thickness due to the high metal thermal diffusivity. Sensitivity to film thickness is strong at high frequency and falls off at lower frequencies. The different behavior of the sensitivities in different ranges is what allows the lateral thermal conductivity and film thickness to be determined simultaneously. For the fused silica substrate (thermal diffusivity $=8.46\times10^{-7}$ m^2/s), sensitivity to the interface conductance is very low, since the low substrate thermal diffusivity is the primary barrier to cross-plane heat flow. For the sapphire substrate (thermal diffusivity $=1.5\times10^{-5}$ m^2/s) the sensitivity to the interface is greater, and the sensitivity to the in-plane thermal conductivity is also reduced because a larger portion of heat is conducted in the substrate. This effect limits this method to the study of films on low-diffusivity substrates.

Although the sensitivity to film thickness is shown in Fig. 5, it is the thermal mass of the metal film ($\rho c_p d$ where ρ is the density, c_p is the specific heat capacity, and d is the film thickness) that is actually affecting the heat flow. This is because there is essentially no temperature gradient across the film. Therefore, from the film thermal mass, if two of the three properties ρ, c_p, and d are known from an independent measurement or are assumed to have the same values as those of bulk solids, the remaining property can be determined. For example, if film thickness is know from picosecond acoustics or profilometry, and assuming c_p is the same as for the bulk metal, we have a way to determine the density of thin metal films. On the other hand, if the film thickness is unknown but the density is close to that of the bulk, film thickness can be determined.

IV. SUMMARY

The FDTR method was applied to the analysis of thin metal films on low thermal diffusivity substrates. Both the thermal mass and thermal conductivity of Au and Al films in the range of 20–100 nm were determined simultaneously from a single measurement. If the film thickness is measured independently, the thermal mass yields the metal film density; if bulk density is assumed then an estimate of film thickness is obtained. From the thermal conductivity and the WF law, the electrical conductivity of the films can be estimated in temperature and size regimes where the law is valid. Outside these regimes, the FDTR technique can be used in conjunction with electrical measurements to explore size effects on thermal and electrical transport in thin films.

ACKNOWLEDGMENTS

The authors would like to thank Ms. Kimberlee Collins for her assistance preparing our samples, and Mr. Austin Minnich for performing the electrical conductivity measurements.

[1] A. Mandelis, Rev. Sci. Instrum. **57**, 617 (1986).
[2] A. Rosencwaig, J. Opsal, W. L. Smith, and D. L. Willenborg, Appl. Phys. Lett. **46**, 1013 (1985).
[3] G. Langer, J. Hartmann, and M. Reichling, Rev. Sci. Instrum. **68**, 1510 (1997).
[4] A. Yarai and T. Nakanishi, Rev. Sci. Instrum. **78**, 054903 (2007).
[5] J. Opsal, A. Rosencwaig, and D. L. Willenborg, Appl. Opt. **22**, 3169 (1983).
[6] E. Ogawa, C. Hu, and P. Ho, J. Appl. Phys. **86**, 6018 (1999).
[7] B. Li, J. Roger, L. Pottier, and D. Fournier, J. Appl. Phys. **86**, 5314 (1999).
[8] B. Li, L. Pottier, J. P. Roger, D. Fournier, and E. Welsch, Rev. Sci. Instrum. **71**, 2154 (2000).
[9] C. A. Paddock and G. L. Eesley, J. Appl. Phys. **60**, 285 (1986).

Downloaded 26 Sep 2011 to 65.96.249.255. Redistribution subject to AIP license or copyright; see http://jap.aip.org/about/rights_and_permissions

[10]W. S. Capinski, H. J. Maris, T. Ruf, M. Cardona, K. Ploog, and D. S. Katzer, Phys. Rev. B **59**, 8105 (1999).
[11]D. G. Cahill, Rev. Sci. Instrum. **75**, 5119 (2004).
[12]S. Huxtable, D. Cahill, V. Fauconnier, and J. White, Nature Mater. **3**, 298 (2004).
[13]A. J. Schmidt, R. Cheaito, and M. Chiesa, Rev. Sci. Instrum. **80**, 094901 (2009).
[14]N. Ashcroft and D. Mermin, *Solid State Physics* (Harcourt College, New York, 1976).
[15]C. Thomsen, H. T. Grahn, H. J. Maris, and J. Tauc, Phys. Rev. B **34**, 4129 (1986).
[16]S. Gurrum, W. King, Y. Joshi, and K. Ramakrishna, ASME J. Heat Transfer **130**, 082403 (2008).
[17]D. Fournier and C. Fretigny, Eur. Phys. J. Spec. Top. **153**, 69 (2008).
[18]A. J. Schmidt, X. Chen, and G. Chen, Rev. Sci. Instrum. **79**, 114902 (2008).
[19]A. Schmidt, M. Chiesa, X. Chen, and G. Chen, Rev. Sci. Instrum. **79**, 064902 (2008).
[20]Q. G. Zhang, B. Y. Cao, X. Zhang, M. Fujii, and K. Takahashi, Phys. Rev. B **74**, 134109 (2006).
[21]X. Zhang, H. Xie, M. Fujii, H. Ago, K. Takahashi, T. Ikuta, H. Abe, and T. Shimizu, Appl. Phys. Lett. **86**, 171912 (2005).

Downloaded 26 Sep 2011 to 65.96.249.255. Redistribution subject to AIP license or copyright; see http://jap.aip.org/about/rights_and_permissions